ELSEVIER

Chemical Geology 217 (2005) 277–293

CHEMICAL GEOLOGY
INCLUDING
ISOTOPE GEOSCIENCE

www.elsevier.com/locate/chemgeo

Experimental evaluation of mixed fluid reactions between supercritical carbon dioxide and NaCl brine: Relevance to the integrity of a geologic carbon repository

John P. Kaszuba[a,*], David R. Janecky[b], Marjorie G. Snow[c]

[a]*Isotope and Nuclear Chemistry, Mail Stop J514, Los Alamos National Laboratory, Los Alamos, NM 87545, USA*
[b]*Risk Reduction and Environmental Stewardship, Mail Stop J591, Los Alamos National Laboratory, Los Alamos, NM 87545, USA*
[c]*Earth and Environmental Sciences, Mail Stop D469, Los Alamos National Laboratory, Los Alamos, NM 87545, USA*

Received 5 May 2003; accepted 10 December 2004

Abstract

The reactive behavior of a mixed fluid (supercritical CO_2 and brine) under physical–chemical conditions relevant to geologic storage and sequestration in a carbon repository is largely unknown. Experiments were conducted in a flexible cell hydrothermal apparatus to evaluate fluid–rock (aquifer plus aquitard) reactions that may adversely impact the integrity of the repository. A 5.5 molal NaCl brine–rock system was held at 200 °C and 200 bars (20 MPa) for 32 days (772 h) to approach steady state, then injected with CO_2 and allowed to react for an additional 45 days (1079 h). In a separate experiment at 200 °C and 200 bars, the system was allowed to react for 77 days (1845 h) without injection of CO_2. Corroded magnesite and euhedral siderite crystallized in a paragenetic sequence after CO_2 injection. Nucleation and growth of siderite on shale suggests the aquitard is a reactive component in the system. Changes in elemental abundances in the brine following addition of CO_2 include pH decrease and depletion of sodium due to accelerated growth of analcime. A pH increase follows pressure and temperature decrease and loss of saturated CO_2 from acidic brine. Silica concentrations and dissolution rates are enhanced and silica precipitation inhibited in the acidic brine.

Geochemical reactions in a carbon repository extend beyond pH decrease and carbonate mineral precipitation. Rock-dominated reaction systems yield to acid-dominated and related reactions controlled by mixed fluid equilibria (i.e., a fluid-dominated system). Escape of CO_2 or migration of brine from the repository into overlying aquifers may cause silica super-saturation and increased alkalinity due to mixed fluid phase equilibria. These geochemical changes could be monitored in aquifers as indicators of repository integrity. Return of silica super-saturated brine to a rock-dominated reaction system buffered to neutral pH conditions may enhance precipitation of quartz, chalcedony, or amorphous silica. In addition to the potential effects (beneficial or deleterious) that silica super-saturation and precipitation may hold for repository performance, an understanding of the effects of multi-phase equilibrium relationships between supercritical CO_2 and dissolved silica in aquifer–brine systems also raises new questions for a variety of geologic systems. Multi-phase fluid

* Corresponding author. Tel.: +1 505 665 7832; fax: +1 505 665 4955.
E-mail address: jkaszuba@lanl.gov (J.P. Kaszuba).

0009-2541/$ - see front matter
doi:10.1016/j.chemgeo.2004.12.014

equilibria may, for example, account for quartz cements in some sedimentary basin sandstones and quartz vein mineralization in some ore districts.

Keywords: Carbon dioxide; Geologic sequestration; Multi-phase fluids; Quartz veins; Crustal fluids

1. Introduction

A promising approach to the problem of managing anthropogenic carbon is to store and dispose carbon dioxide into geologic formations, including saline aquifers, depleted petroleum reservoirs, and coal deposits. These formations have contained fluids, including natural gas, coal bed methane, and naturally occurring carbon dioxide, for geologic time and possess a capacity sufficient for disposal of many decades or centuries worth of anthropogenic carbon dioxide (Koide et al., 1992). In addition, these formations are widely available and in close proximity to power generation plants (Hitchon et al., 1999), a major source of carbon dioxide emissions (Holloway, 1997).

Geologic formations artificially charged with carbon dioxide are here defined as a *carbon repository*. The carbon repository is a complex structural and stratigraphic package containing diverse geochemical environments, brine and groundwater chemistries, sandstone and shale compositions, lateral facies transitions, etc. Overlying confining beds (aquitards) must also be considered as a part of this potentially rich reaction environment, the stability of which are critical to long-term containment of carbon dioxide. The environment of a carbon repository would also span a range of depths for initial emplacement and subsequent migration, and therefore a range of pressures and temperatures of geochemical interest. Pressures may range from a few bars where carbon dioxide has migrated to the near-surface to several hundreds of bars within the initial zone of emplacement. Temperatures may range as high as 150–200 °C, depending on local and regional geothermal gradients (Bachu, 2002, 2003). Within this environment, carbon dioxide will be in the supercritical state, because its critical point lies at approximately 31 °C and 74 bars (Span and Wagner, 1996), and will be immiscible in water (Takenouchi and Kennedy, 1964).

Emplacement of carbon dioxide into a carbon repository and the mechanisms for retention therein are discussed in detail elsewhere (Bachu et al., 1994). Broadly speaking, mineral precipitation can be referred to as sequestration, whereas stratigraphic and/or structural trapping and hydrodynamic trapping can be termed storage. Sequestration, therefore, implies the tying up of carbon in a geologically stable form, whereas storage implies a potentially shorter-term method.

Far less attention has been paid to mechanisms that adversely impact the integrity of a carbon repository. Lindeberg (1997) was among the first to quantitatively evaluate escape mechanisms of carbon dioxide emplaced in a saline aquifer. With simple numerical models incorporating the Darcy equation and Fick's law, Lindeberg (1997) attributed leakage of carbon dioxide to gravity migration with subsequent release through subvertical fractures and faults. More recently, numeric simulations were used to evaluate injection of carbon dioxide into a brine aquifer and calculate the potential for leakage by discharge along a fracture or fault zone (Ennis-King and Paterson, 2000; Pruess and Garcia, 2002; Saripalli and McGrail, 2002) and by caprock failure (Rutqvist and Tsang, 2002). These simulations did not evaluate the effects of geochemical reactions (positive or negative) on injection and leakage of carbon dioxide.

A few experimental studies do examine geochemical reactions in a saline aquifer in response to injection of carbon dioxide under repository conditions. In numerical geochemical modeling studies that incorporate kinetic rate laws (Gunter et al., 2000; Perkins and Gunter, 1995) and one study combining experiment and modeling (Gunter et al., 1997), dissolution of silicate minerals in a brine and precipitation of carbonate are reported. In their investigation, Kaszuba et al. (2003) identified geochemical reactions within an experimental system at reservoir temperature and pressure and began to identify potential failure modes due to geochemical mechanisms.

The purpose of this study is to evaluate an experimental brine–rock (aquifer plus aquitard) system

that simulates a carbon repository for fluid–rock reactions that may adversely impact the integrity of the repository. Geochemical behavior of multiphase and supercritical CO_2 fluid in this system will defy simplistic field sampling, assumptions and predictions because the reactions will involve a two-phase fluid (supercritical carbon dioxide and brine). Therefore, evidence for fluid–rock reactions that may be detrimental to the repository include experimental data, natural reaction textures on minerals comprising the aquitard, and deleterious changes in brine chemistry. A carbon repository will exhibit a wide range of temperature and pressure, approximately 50–200 °C and 20–1000 bars (Bachu, 2000; Benson, 2000; Carter et al., 1998; Hitchon et al., 1999; Hurter and Pollack, 1996; Oldenburg et al., 2001). The relatively high temperature of 200 °C was selected for this study for consistency with the experimental work of Kaszuba et al. (2003) and so that kinetic rates of silicate reactions would be maximized. A pressure of 200 bars (20 MPa) was chosen for consistency with Kaszuba et al. (2003) and accessibility for sequestration scenarios. In contrast to the brine used by Kaszuba et al. (2003), in which Na, Mg, and K were the predominant cations and Cl the predominant anion, NaCl brine was used as the initial fluid to emphasize reactions in the rock. Thus, the brines evaluated by Kaszuba et al. (2003) and in this work present a range of reaction potential among rock, brine, and supercritical CO_2. On one hand, carbonate mineral may readily precipitate from Mg-rich brine containing aqueous carbonate ion buffered by coexisting supercritical CO_2 (Kaszuba et al., 2003). On the other, the Na-rich brine, initially devoid of divalent cations, can only derive the cations needed for carbonate precipitation by reaction with silicate minerals.

Evidence for reactions involving the aquitard and potentially deleterious changes in brine chemistry were observed in our experiments, from which a number of clear implications can be drawn regarding the integrity of a carbon repository. The discussion is also extended to other geochemical systems in which supercritical carbon dioxide may have impact.

2. Material and methods

2.1. Experimental approach

A model aquifer–aquitard geochemical system was reacted with brine at 200 °C and 200 bars (20 MPa)

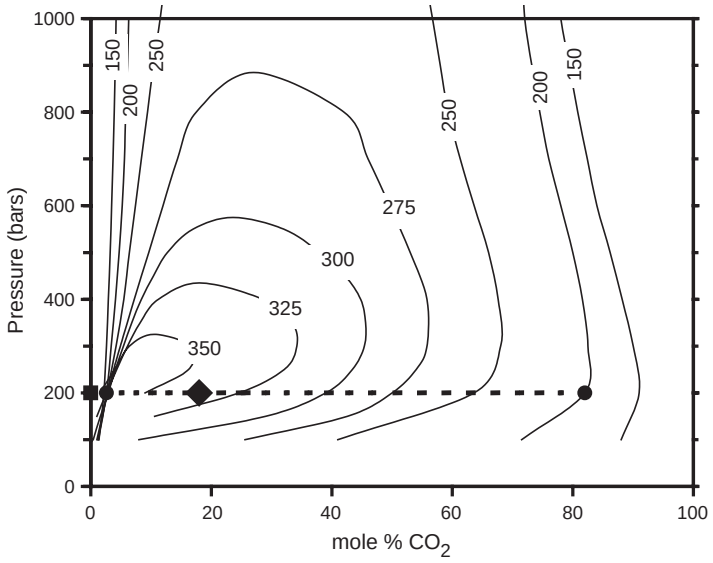

Fig. 1. Pressure-X_{CO2} phase diagram for H_2O+CO_2 with consolute curves for temperatures of 150 to 350 °C (after Takenouchi and Kennedy, 1964). Bulk compositions of the experimental reactions for brine–rock (square) and supercritical CO_2–brine–rock after injection of CO_2 (diamond) are also plotted. The dashed line represents the phase relationships specific to the supercritical CO_2–brine–rock experiment at 200 °C and 200 bars (20 MPa).

for 32 days (772 h) to approach steady state with respect to major element concentrations. Carbon dioxide was then injected into the system and the experiment continued for another 45 days (1079 h). At 200 °C and 200 bars, carbon dioxide in the reaction cell is a supercritical fluid that is largely immiscible, but not totally insoluble, in brine (Fig. 1) and free to react with the aquifer–aquitard–brine system. To provide a basis of understanding for the effect of the two fluids in this experiment, a separate brine–rock experiment was allowed to react for 77 days (1845 h) at 200 °C and 200 bars and without injection of carbon dioxide. Brine was periodically sampled and analyzed during both experiments. After the experiments were terminated, the solids and quenched brine were analyzed.

2.2. Experimental apparatus

The experiment was conducted in a flexible cell hydrothermal apparatus consisting of a gold–titanium reaction cell contained within a steel pressure vessel (Seyfried et al., 1987). The cell is plumbed to a valved capillary tube that serves as a sampling port. This equipment allows fluid samples to be withdrawn from the gold reaction cell at the temperature and pressure of an experiment and to be rapidly cooled to ambient conditions in less than a few seconds. Consequently, retrograde reactions with minerals that may occur during a prolonged quench process are avoided and solution composition can be analyzed along a reaction pathway. Fluids such as carbon dioxide can also be introduced into the reaction cell during an experiment to allow external modification of the fluid composition (Kaszuba et al., 2003). This equipment also allows external control and monitoring of temperature and pressure. Estimated maximum temperature and pressure uncertainty was ±2 °C and ±5 bars, respectively. Once the experiments stabilized after the first 72 h, fluctuations of <2 °C and ≤7 bars occurred over the course of the experiments.

2.3. Materials

Arkose was chosen as the geochemical and mineralogical representation of an aquifer for these experiments because it provides a diverse geochemical reaction basis and commonly occurs as the reservoir host in sedimentary basins. The arkose was constructed from equal amounts of naturally occurring Minas Gerais quartz, oligoclase ($An_{17–21}$), and microcline ($Or_{91–97}$) exhibiting perthitic exsolution ($Or_{3–9}$). The quartz and oligoclase grains are angular mineral fragments that range in size from 1 to 5 mm. Microcline is also angular in shape but is smaller in size, ranging from approximately 0.5 to 1 mm. Biotite was added as a proxy for ferromagnesium minerals that occur in arkoses. Biotite grains range in size from approximately 0.1 to 1 mm.

A sample from the Silurian Maplewood Shale, an argillaceous shale from Monroe County, New York, USA, was selected as a geochemical representation of an aquitard. The shale is specimen #52 from the Ward's collection of North American Rocks (Ward's Natural Science Establishment, 1970). Examination of the shale using optical and scanning electron micro-

Table 1
Chemical composition of Maplewood Shale

	%	
SiO_2	60.66	(0.72)
TiO_2	0.84	(0.02)
Al_2O_3	17.78	(0.26)
Fe_2O_3	4.82	(0.07)
MnO	0.03	(0.01)
MgO	2.32	(0.06)
CaO	0.78	(0.11)
Na_2O	0.19	(0.12)
K_2O	5.88	(0.08)
P_2O_5	0.12	(0.01)
LOI	5.11	
Total	93.43	
	ppm	
V	110.0	(14.7)
Cr	90.8	(10.0)
Ni	32.6	(11.4)
Zn	61.3	(10.7)
Rb	218.4	(12.4)
Sr	88.5	(5.4)
Y	37.1	(9.0)
Zr	126.3	(10.2)
Nb	19.8	(7.4)
Ba	364.5	(46.3)
Total trace elements (%)	0.14	
Total elements (%)	93.57	
Total elements+LOI	98.68	

Analysis by X-ray fluorescence.
LOI=loss on ignition.
Maximum 2σ uncertainty in parentheses.

Table 2
Water chemistry (mmol/kg), brine–rock experiment, 200 °C, 200 bars

Time (h)	pH	Na	K[a]	Ca[a]	Mg[a]	Cl	Br	SO_4	SiO_2[a]	Al[a]	Fe	Mn	B[a]
Initial brine	8.00	4852	0.19	0.07	0.009	4865	<0.06	<0.1	0.06	0.005	<0.002	<0.0004	0.19
335	5.92	4135	2.38	2.84	0.074	4183	<0.06	<0.1	2.46	0.015	0.061	0.012	0.07
671	5.91	4239	2.63	2.99	0.047	4099	<0.06	<0.1	2.49	0.007	0.005	0.013	0.21
1007	5.86	4257	3.45	3.27	0.057	4397	<0.06	0.09	2.48	<0.004	0.004	0.014	0.27
1841	5.80	4200	3.99	3.67	0.062	4411	<0.06	0.09	2.57	<0.004	0.008	0.019	0.21
Quench													
1845	5.95	4148	3.94	3.67	0.074	4294	<0.06	0.09	2.42	<0.004	0.010	0.020	0.17
Maximum 2σ uncertainty[c]	4%	1%	6%	1%	1%[b]	5%	5%	5%	1%	12%[b]	2%	2%[b]	1%[b]

[a] Laboratory-grade NaCl salt was used to synthesize the brine. Low concentrations of ions other than Na or Cl measured in the initial brine are from impurities in the NaCl salt (e.g., K and B).
[b] Higher analytical uncertainty for trace constituents in initial brine (4% for Mg, 20% for Al, 3% for B) and for sample at 1007 h (4% for Mg and 5% for Mn).
[c] Excluding pH, charge balance is within 96% for all analyses except initial brine and sample at 671 h, which balance to within 99%.

scopy and X-ray diffraction identified clay minerals (10-Å phyllosilicates illite and mica comprising 65 vol.% of the shale), quartz (27%), feldspar (5%), chlorite (2%, may include some kaolinite), and trace quantities of framboidal pyrite. Mineral grains range in size from approximately 2 to 15 μm. The chemical composition of the shale is presented in Table 1. For use in the experiments, the shale was broken into angular fragments approximately 0.5 to 1.5 cm in largest dimension.

NaCl brine (Tables 2 and 3) was synthesized using standard laboratory-grade salt. The ionic strength (5.5 molal) matches the brine used by Kaszuba et al. (2003). The latter brine was modeled after naturally occurring saline aquifers in the Delaware Basin of southeastern New Mexico (Stein and Krumhansl, 1988). Delaware Basin brine represents an extreme natural chemistry that maximizes mineral precipitation from the brine itself.

The supercritical carbon dioxide–brine–rock experiment was performed in a gold reaction cell (108 cm^3) loaded with 3.1 g of arkose (1:1:1:0.3 quartz/plagioclase/microcline/biotite), 2.7 g of Maplewood Shale chips, and 90 g of brine. Following extraction of 33.3 g of brine as samples during the initial 771 h of reactions, approximately 6 g of carbon dioxide was

Table 3
Water chemistry (mmol/kg), supercritical carbon dioxide–brine–rock experiment, 200 °C, 200 bars

Time (h)	pH	Na	K	Ca	Mg	Cl	Br	SO_4	SiO_2	Al	Fe	Mn	B	$\sum CO_2$
Initial brine	8.00	4851	<0.13	0.02	0.02	5098	<0.06	<0.1	<0.04	<0.04	<0.01	<0.002	0.03	0.09
339	6.07	4339	2.51	2.64	0.25	4253	<0.06	0.4	2.10	<0.04	0.045	0.011	0.10	–
771	5.83	4112	2.56	3.42	0.45	4233	<0.06	<0.1	2.91	<0.04	0.011	0.013	0.35	5.2
Inject CO_2														
772	–	–	–	–	–	–	–	–	–	–	–	–	–	–
842	6.57	4007	2.52	3.94	3.47	4142	<0.06	<0.1	5.34	<0.04	0.94	0.067	0.40	269
1011	6.68	3886	2.61	3.87	4.05	4145	<0.06	<0.1	5.52	<0.04	1.22	0.057	0.26	301
1179	6.46	3984	2.81	3.74	3.98	3899	<0.06	<0.1	5.55	<0.04	1.02	0.055	0.18	240
1850	6.62	3600	2.97	4.12	3.88	4006	<0.06	0.2	7.72	<0.04	0.885	0.054	0.30	271
Quench														
1851	–	3639	2.99	4.12	4.12	3924	<0.06	0.2	6.73	<0.04	0.577	0.058	0.14	–
Maximum 2σ uncertainty[a]	4%	2%	7%	1%	2%	5%	5%	5%	3%	NA	2%	5%	7%	10%

[a] Analytical uncertainty in analysis of the initial brine is 7% for Ca, 42% for Mg, and 30% for B. Excluding pH, charge balances within 95% for all analyses except final sample (1850 h and quench sample), which balance within 90%.

injected into the reaction cell. Thus, the initial brine to rock mass ratio was 15.5:1 and the initial brine to carbon dioxide mass ratio was approximately 9.5:1. The brine–rock experiment was performed in a smaller titanium reaction cell (79 cm^3) loaded with 2.2 g of arkose (1:1:1:0.3 quartz/plagioclase/microcline/biotite), 1.9 g of Maplewood Shale chips, and 64.1 g of brine. The initial brine to rock mass ratio for this experiment was also 15.5:1. No attempt was made to control the redox state of either experiment.

2.4. Analytical methods

Hydrothermal fluids within the reaction cell were sampled as described by Seyfried et al. (1987). Brine samples were diluted (10×) and divided into two subequal fractions for cation and anion analysis. To prevent precipitation, the aliquot of brine for cation analysis was acidified to pH 2 with nitric acid. Dissolved Si, Ca, Mg, Na, K, and B were determined by ICP-ES, dissolved Al, Fe, and Mn by ICP-MS, and dissolved anions by ion chromatography. Separate aliquots of brine were used for analysis of total carbon (as carbon dioxide) by coulometric titration (Huffmann, 1977). Mineral precipitates were not observed in any of the samples. Analytical results and uncertainties are reported in Tables 2 and 3. Solids were analyzed using optical microscopy and scanning electron microscopy (SEM). Secondary and backscattered electron signals and qualitative X-ray analysis using Energy Dispersive Spectrometry (EDS) were used in SEM analysis.

3. Experimental results

3.1. Brine chemistry during reactions

Initial fluctuations observed in brine chemistries, as recorded in the first fluid samples collected at approximately 340 h (Tables 2 and 3), reflect adjustment of brine to rock. Concentrations of Na and Cl in the brines decrease by approximately 15% (Fig. 2). Initial pH (measured as 8 at 25 °C and calculated as 5.5 at 200 °C, Fig. 3) decreased by approximately 0.6 units (2 units in the sample measured at 25 °C). Trace ions previously absent from NaCl brine appeared in solution at millimolal (K, Ca, and SiO_2) to micromolal (Mg, Al, Fe and Mn) quantities (Figs. 4 and 5).

In the brine–rock experiment, the initial decrease of the Na concentration is followed by a 2.5% increase at 671 h (Table 2, Fig. 2). The Na concentration subsequently decreases for the duration of the experiment. Although this decrease falls within the analytical uncertainty, our interpretation of Na

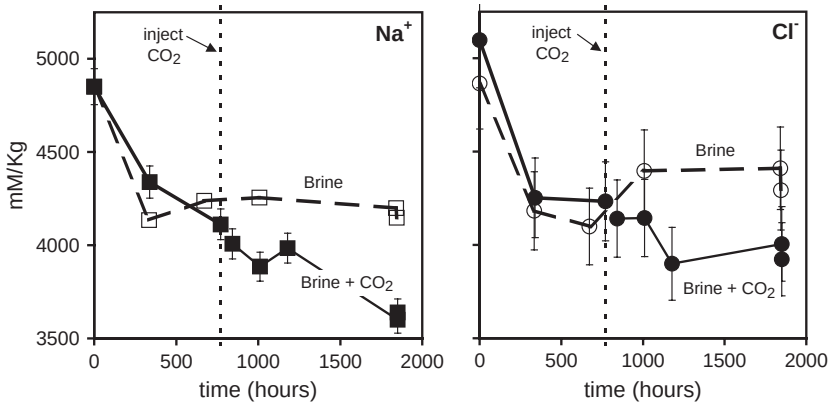

Fig. 2. Brine chemistry as a function of time for sodium (figure at left) and chloride (figure at right) during the experimental reaction for brine–rock (open symbols and dashed lines) and supercritical CO_2–brine–rock (solid symbols and lines). The initial brine to rock mass ratio in both experiments was 15.5:1. Carbon dioxide was injected into the reaction cell of the supercritical CO_2–brine–rock experiment (6 g CO_2 into 56.7 g brine) at 772 h (vertical dashed line) to produce a fluid to rock ratio of ~10:1:1 for brine/CO_2/rock. A two-phase fluid (brine+supercritical CO_2) was also formed. Uncertainties for sodium in the brine–rock experiment are smaller than the size of the symbols. Error bars represent uncertainties for sodium in the supercritical CO_2–brine–rock experiment and for chloride. Samples collected after each experiment was terminated are represented by the last symbol shown for each analyte.

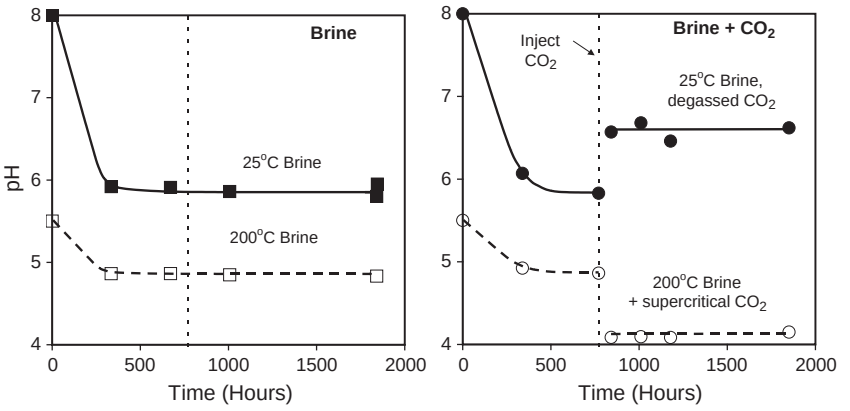

Fig. 3. Interpretation of pH behavior during the experimental reaction for brine–rock (figure at left) and supercritical CO_2–brine–rock (figure at right). For both experiments, pH is measured at 25 °C, 1 bar in samples from which CO_2 has degassed to atmospheric saturation (solid lines and symbols). Changes in the pH of the brine in response to increased temperature (200 °C) and CO_2-saturation (Table 2) were calculated sequentially using Geochemist's Workbench 3.1 and the b-dot ion association model (Bethke, 2000) to determine an in-situ pH (dashed lines and open symbols). In both experiments, in-situ pH decreases from 5.5 to 4.9 by the time the first sample is collected. Following injection of CO_2 into the supercritical CO_2–brine–rock experiment, in-situ pH further decreases to approximately 4.1 (open circles). At 25 °C, pH measured in brine from this experiment, after CO_2 is injected, is approximately 6.6 (solid circles). Uncertainties (0.2 pH units) are equal to the size of the symbols.

decrease is consistent with the precipitation of analcime as discussed in the next section. At the rate of decrease observed in the final 800 h of the experiment, an additional 1000 h would be needed to determine the Na decrease beyond the limits of uncertainty. The initial Cl decrease is followed by a 2% decrease at 671 h and a 7% increase at 1007 h. These changes, however, are within the 5% uncertainty of Cl analyses. After 1007 h, the Cl concentration remained stable for the duration of the experiment. After the initial pH decrease, the in-situ pH of approximately 4.8 (measured pH of approximately 5.9) remained stable for the duration of the experiment (Fig. 3). The stabilization of Na and Cl concentrations and pH suggests that the brine achieved an approximate steady state with respect to the major elements and pH, controlled by the alteration mineral assemblage.

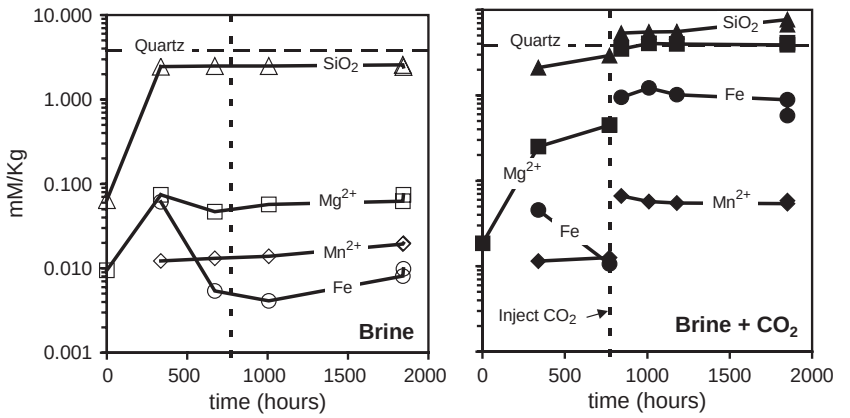

Fig. 4. Brine chemistry as a function of time for SiO_2 (triangles), Mg (squares), Mn (diamonds), and Fe (circles) during experimental reaction of brine–rock (figure at left) and supercritical CO_2–brine–rock (figure at right). The vertical dashed line at 772 h indicates injection of carbon dioxide into the reaction cell of the supercritical CO_2–brine–rock experiment (figure on right). The vertical dashed line is repeated in the figure on the left (brine–rock experiment) for reference. Horizontal dashed line is calculated quartz solubility. Uncertainties are smaller than the size of the symbols. Samples collected after each experiment was terminated are represented by the last symbol shown for each analyte.

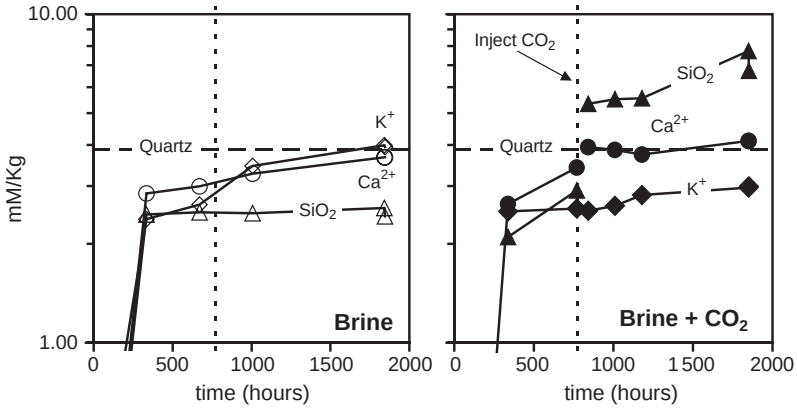

Fig. 5. Brine chemistry as a function of time for Ca (circles) and K (diamonds) during experimental reaction of brine–rock (figure at left) and supercritical CO_2–brine–rock (figure at right). Calculated quartz solubility (horizontal dashed line) and SiO_2 (triangles) from Fig. 3 are plotted for reference. Uncertainties are smaller than the size of the symbols. Ca and K in samples collected after each experiment was terminated are nearly identical to the last sample collected at pressure and temperature.

In contrast to Na, Cl, and pH, the concentrations of trace elements did not stabilize in the latter stages of the brine–rock experiment (Tables 2 and 3, Figs. 4 and 5). Because these ions are present in trace amounts, they may be indicators of more subtle changes in the alteration mineral assemblage. After the 335-h sample, the SiO_2 concentration was stable to 1007 h, then increased by approximately 4% in the final sample (1841 h). These SiO_2 concentrations are below the calculated solubility of quartz. The Mg concentration decreased between 335 and 671 h, then increased throughout the duration of the experiment, although the apparent rate of increase diminishes in the latter portion of the experiment. The Mn concentration increased throughout the duration of the experiment, and the apparent rate of increase was greatest between the last two samples collected. The Fe concentration decreased between 335 and 1007 h, after which it increased. The Ca and K concentrations increased throughout the duration of the experiment.

In the time preceding injection of CO_2 into the supercritical CO_2–brine–rock experiment (the first 771 h), pH and concentrations of Na, Cl, and trace elements were similar to concentrations in the initial 770 h of the brine–rock experiment (Tables 2 and 3, Figs. 2–5). The exception is Mg, with concentrations 3 to 10 times larger than observed in the brine–rock experiment. In the initial stages of the experiments, Mg is dissolving out of rock and entering a solution that is initially Mg free. The micromolal concentrations of Mg are likely controlled by detailed mineral dissolution kinetics, and not yet by secondary mineral solubility, therefore these differences are not surprising.

Injection of approximately 6 g of CO_2 into the reaction cell of the supercritical CO_2–brine–rock experiment at 772 h increased the pressure of the experimental system from 196 to 254 bars. The pressure decreased by a total of 24 bars over the following 39 h. The system pressure subsequently stabilized at approximately 230 bars for the duration of the experiment, with fluctuations of a few bars that were correlated to ambient temperature changes in the laboratory and experimental apparatus. The pressure was not readjusted to 200 bars to emulate the effect of adding supercritical CO_2 to a pressurized aquifer system. The 24 bar pressure decrease is consistent with previously observed behavior (Kaszuba and Janecky, 2000; Kaszuba et al., 2003).

Injection of CO_2 into the supercritical CO_2–brine–rock experiment also produced significant changes in the brine, changes that are apparent by comparing the brine chemistry between the two experiments. Na and Cl concentrations and pH decreased, as measured in the sampling event held 70 h after injection of CO_2 (Tables 2 and 3, Figs. 2 and 3). The concentration of Na continued to decrease and did not stabilize. The concentration of Na in the sample collected immediately prior to termination of the experiment was approximately 12% less than the Na concentration of the sample collected 1 h before injection of CO_2 and

14% less than the Na concentration of the brine–rock experiment. The concentration of Cl decreased by approximately 8% until 1179 h (407 h after CO_2 injection), then stabilized at a concentration approximately 11% less than that of the brine–rock experiment. The apparent late increase in Cl concentration (compare data between 1179 and 1850 h) is within the 5% uncertainty for anion analyses (Table 3). The in-situ pH abruptly decreased to approximately 4.1, a pH that is 0.7 units lower than observed in the brine–rock experiment, and stabilized for the duration of this experiment. At 25 °C, the pH measured in degassed brine from this experiment rebounded to approximately 6.6. This pH is approximately 0.8 units higher than the pH measured in brine samples from the final 1000 h of the brine-experiment.

In contrast to changes in Na and Cl concentrations and pH, most trace element concentrations abruptly increased (Ca, 15%; Mg, 8×; SiO_2, 80%; Fe, 100×; and Mn, 5×) in the first sample collected (842 h) after CO_2 was injected (Tables 2 and 3, Figs. 4 and 5). The K concentration exhibited no measurable change in this same interval. The Ca concentration decreased by 5% from 842 to 1179 h, then increased by 10% for the duration of the experiment. Ca concentrations increased in the latter stages of both experiments but are 12% to 18% higher in the supercritical CO_2–brine–rock experiment. Concentrations of Mg and Fe increased by 15% and 30%, respectively, from 842 to 1011 h, then decreased by approximately 4% to 30% for the duration of the experiment. In contrast to the brine–rock experiment, the Mg and Fe concentrations were approximately an order of magnitude greater and decreased in the latter stages of the experiment. The SiO_2 concentration increased by 3% from 842 to 1011 h (70 to 239 h after injecting CO_2). It remained stable until 1179 h (407 h after injecting CO_2) at a concentration approximately twice that of the brine–rock experiment, then increased by 40% for the duration of the experiment. The rate of increase of SiO_2 concentration is approximately 30 times greater compared to the brine–rock experiment. Unlike the brine–rock experiment, SiO_2 concentrations are greater than the calculated solubility of quartz. The Mn concentration decreased by a total of 20%, whereas the K concentration increased by a total of 18% between 842 h and the termination of the experiment. The Mn concentrations were approximately 5 times greater and decreased throughout the latter stages of this experiment as compared to the brine–rock experiment. While the K concentrations increased in both experiments, they are approximately 30% less in this experiment. K is the only trace element in this experiment that is present in smaller amounts than in the brine–rock experiment. The significant increase in concentration of most trace elements suggests the rock dissolved by reaction with CO_2 and brine, behavior consistent with the in-situ pH decrease and increased CO_2 dissolved in brine due to carbon dioxide injection. The pressure drop observed in the reaction system, therefore, appears to be an external measure of the overall supercritical CO_2–brine–rock reaction rate for this process.

Concentrations of several of the ions in brine samples collected after the experiment were terminated were different from concentrations in samples collected immediately prior to termination. In the brine–rock experiment, the SiO_2 concentrations were smaller by 6%, whereas Mg (19%), Fe (25%), and Mn (5%) concentrations were greater. In the supercritical CO_2–brine–rock experiment, SiO_2 (13%) and Fe (35%) concentrations were smaller, whereas Mg (6%) and Mn (7%) concentrations were greater. Na, K, Ca, and Cl concentrations exhibited no change in either experiment.

3.2. Reaction of solid phases

While carbonate minerals did not precipitate in the brine–rock experiment, two types of carbonate minerals precipitated in the supercritical carbon dioxide–brine–rock experiment. Magnesite occurs as large (up to several mm in length), discrete, bladed crystals visible to the naked eye (Fig. 6). The crystal faces of the magnesite are pitted and rough, suggesting that magnesite was undersaturated at the time the experiment was terminated. Siderite occurs as euhedral crystals, about 200–250 μm in diameter, on the shale (Fig. 7). The euhedral texture suggests that siderite was an equilibrium phase at the time the experiment was terminated. Qualitative X-ray analysis using EDS confirmed the identification of both minerals, and neither was present in the mineral assemblage at the beginning of this experiment. Therefore, we interpret the carbonate mineral assemblage as precipitation of

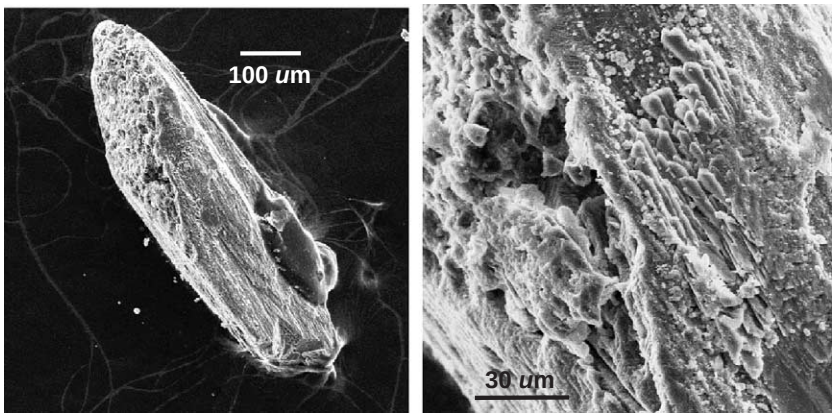

Fig. 6. Secondary electron SEM micrograph of magnesite (figure on left) from the supercritical CO_2–brine–rock experiment. Magnesite crystals are large, up to a few mm in length, and occur as individual grains and splays. Close-up view (figure on right) illustrates pitted crystal faces, indicative of undersaturation and interpreted as dissolution of early-formed magnesite.

magnesite after injection of carbon dioxide, followed by magnesite dissolution and siderite precipitation.

Silicate alteration phases observed are clay minerals and analcime. Secondary clay minerals are present in abundance on surfaces of minerals comprising the arkose and the shale. Analcime trapezohedrons are ubiquitous to both experiments (Figs. 7 and 8) as euhedral crystals, 20–40 μm in diameter, occurring on the shale as well as the minerals comprising the aquifer. Euhedral analcime is more abundant in the brine–rock experiment as compared to the supercritical CO_2–brine–rock experiment. Euhedral textures suggest that analcime crystallized as an equilibrium phase in both experiments. Analcime also occurs as masses of skeletal crystals in the supercritical CO_2–brine–rock experiment, ranging in size from 80 to 120 μm in diameter (Fig. 9). Skeletal textures are interpreted as indicating acceleration of normal crystal nucleation and growth, possibly due to acidity in the brine or to the presence of an immiscible supercritical carbon dioxide phase.

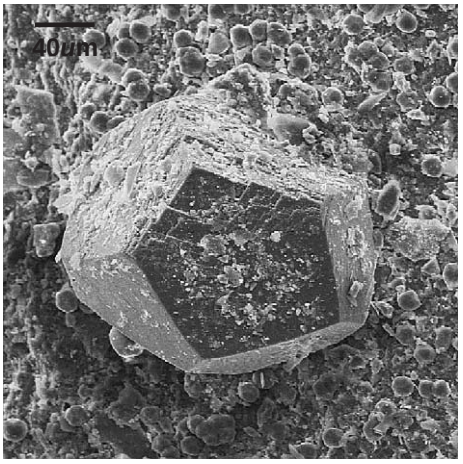

Fig. 7. Secondary electron SEM micrograph of siderite from the supercritical CO_2–brine–rock experiment. Siderite occurs as individual crystals, about 200–250 μm in diameter, growing on shale. Euhedral texture, indicative of equilibrium, is interpreted as precipitation of siderite after early-formed magnesite. Small, rounded grains surrounding the siderite are euhedral analcime.

4. Discussion

4.1. Mixed fluid reactions and processes

In agreement with models proposed for geologic sequestration of carbon (e.g., Gunter et al., 2000), addition of supercritical carbon dioxide into the experimental brine–rock (aquifer plus aquitard) system decreased brine pH and precipitated carbonate minerals. The pressure decrease following injection of carbon dioxide indicates a decrease in the volume of the system due to the phase change of supercritical carbon dioxide, to dissolved carbonate, to mineral carbonate. In addition to pH decrease and carbonate mineral precipitation, a diversity of other fluid–rock reactions took place between the mixed fluid (immiscible supercritical carbon dioxide plus brine, Fig. 1) and rock that differ from the brine–rock system.

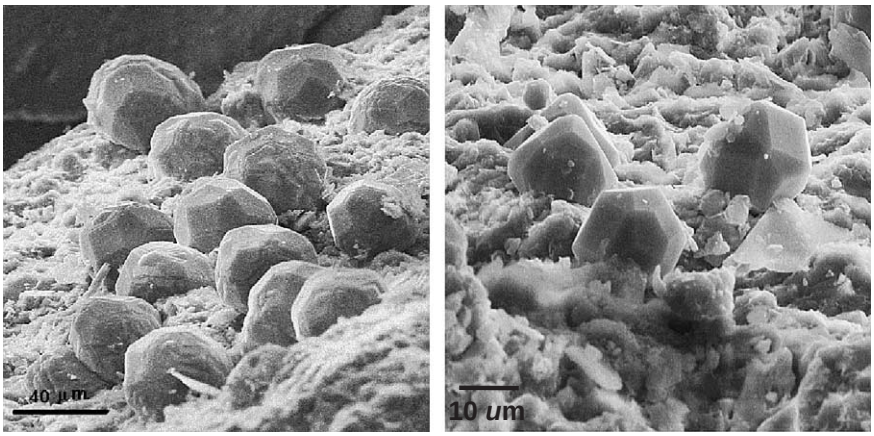

Fig. 8. Secondary electron SEM micrograph of analcime on shale from experimental reaction of brine–rock (figure at left) and supercritical CO_2–brine–rock (figure at right). Euhedral analcime crystals, 20–40 μm in diameter, occur on the shale and the aquifer minerals and are more abundant in the brine–rock experiment as compared to the supercritical CO_2–brine–rock experiment. Euhedral textures are interpreted as equilibrium crystallization.

Supercritical carbon dioxide supplied carbonate to buffer the fugacity of aqueous carbonate and hence the pH of brine in the experimental system. The ability of an actual siliciclastic aquifer to buffer acidity and control geochemical reactions (i.e., a rock-dominated system) may yield to acid-dominated and related reactions controlled by mixed fluid equilibria (i.e., a fluid-dominated system). Adding to the complexity is the pH increase following pressure and temperature decrease and the accompanying loss of saturated carbon dioxide from acidic brine. For a brine–rock system into which supercritical carbon dioxide is catastrophically introduced, whether by anthropogenic injection from above or geologic emplacement from below, the sudden perturbation of on-going reactions may profoundly change the manner in which the geochemistry of the system ultimately evolves.

Acidified brine reacted with biotite and shale (Kaszuba et al., 2003) to immediately enrich the brine in Mg (74×), Fe (188×), and Mn (5×) relative to the brine–rock system (Fig. 4). Subsequent precipitation of carbonate mineral decreased concentrations of these elements in the brine,

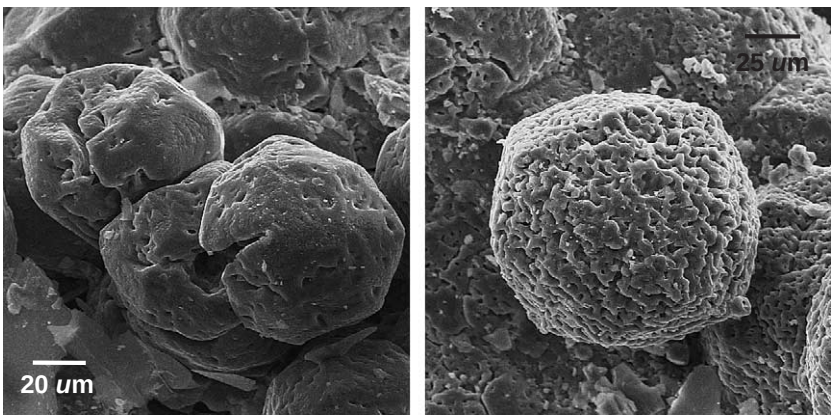

Fig. 9. Secondary electron SEM micrograph of skeletal analcime from experimental reaction of supercritical CO_2–brine–rock. Skeletal analcime crystals, ranging in size from 80 to 120 μm in diameter, occur in crystalline masses. Skeletal textures are interpreted to indicate rapid crystal nucleation and growth, possibly due to acidity in the brine or to the presence of an immiscible supercritical CO_2 phase.

although the concentrations remained greater (Mg, 63×; Fe, 110×; and Mn, 3×) than in the brine–rock experiment. In contrast, reactions in the brine–rock experiment continued to add Mg, Fe, and Mn into solution as the rock reacted to equilibrate with NaCl brine. Without supercritical carbon dioxide and acidified brine, it is unknown whether concentrations of Mg, Fe, and Mn would converge in the two experiments. However, slight differences in minerals, reactive surfaces, and assemblages exposed to the brine, could explain the divergence between experiments.

Sodium and potassium concentrations, as well as steady state chloride concentrations, decreased in acidified brine (Figs. 2 and 5). Although sodium concentrations are also decreasing in the brine–rock experiment, and euhedral analcime precipitates in both systems, the rate of sodium decrease is approximately 10 times greater in the supercritical carbon dioxide–brine–rock experiment (Fig. 10). Crystallization of analcime that is 2 to 6 times larger than early-formed analcime and exhibits skeletal texture presumably accounts for the rapid rate at which the concentration of sodium in the brine decreases. Whether large crystal size and skeletal texture is the result of accelerated growth in acidic brine or to the presence of immiscible supercritical carbon dioxide is not constrained by our experiments. However, it is clear that fluid–rock reaction rates are accelerated and analcime stability enhanced in an acidified brine–supercritical carbon dioxide system. The disposition of potassium is also not constrained by our experiments, although growth of clay minerals (smectite) on biotite and shale (Kaszuba et al., 2003) may account for the decreased potassium concentration.

Silica concentrations are enhanced in the mixed-phase brine by a factor of two as compared to the brine–rock system, at a concentration comparable to the calculated solubility of chalcedony (Fig. 10). And while both systems initially exhibit steady state silica concentrations followed by increasing silica concentration, the rate of increase is approximately 30 times greater in the supercritical carbon dioxide–acid brine system. Clearly, fluid–silicate reaction rates are accelerated and silica solubility is enhanced in an acidified brine–supercritical carbon dioxide system.

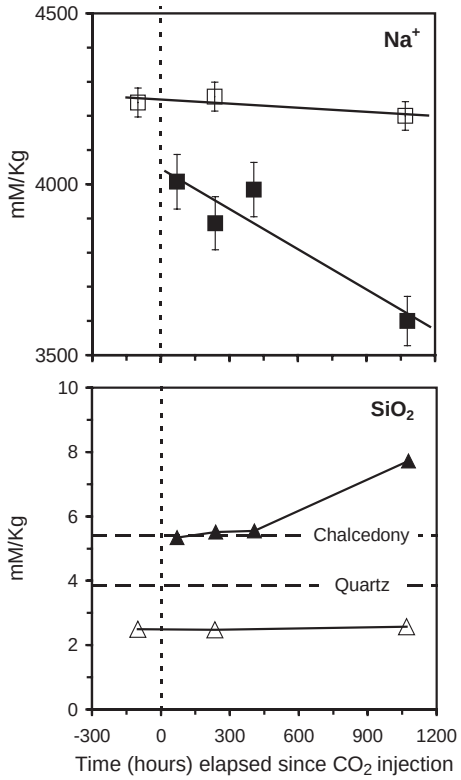

Fig. 10. Relative rate of change of Na (top) and SiO_2 (bottom) concentration as a function of time elapsed since injection of CO_2 into reaction cell. Experimental reaction for brine–rock (open symbols) and supercritical CO_2–brine–rock (solid symbols). Carbon dioxide was injected into the reaction cell of the supercritical CO_2–brine–rock experiment at 0 h (vertical dashed line). Compared to the brine–rock experiment, Na concentration in the supercritical CO_2–brine–rock experiment decreases ~10×, whereas SiO_2 concentration increases ~30×. Horizontal dashed lines are calculated solubility of chalcedony and quartz. Linear regression drawn through Na data, whereas SiO_2 data are connected by line drawn between individual points. Uncertainties for Na analyses shown as error bars. Uncertainties for SiO_2 analyses are approximately the thickness of the line connecting the data points.

4.2. Integrity of a carbon repository

In addition to dissolution of supercritical carbon dioxide into brine, pH decrease, and carbonate mineral precipitation, this study demonstrates that additional geochemical reactions and processes take place between the two-phase fluid (supercritical carbon dioxide and brine) and the aquitard as well as the aquifer minerals. These reactions may give rise to a number of geochemical and geotechnical consequences of significance to a carbon repository.

Increased acidity of the aqueous fluids within a carbon repository is a widely recognized and acknowledged consequence of carbon dioxide disposal (e.g., Gunter et al., 2000). The potential for other reactions that may accompany migration of this fluid within the repository, however, has not been addressed. A pH increase accompanied the loss of saturated carbon dioxide from acidic brine within the experimental system (Fig. 3). With movement of acidic brine to higher stratigraphic levels in a carbon repository, or leakage into overlying strata, water–rock reactions more characteristic of lower temperature, lower pressure, and neutral or even alkaline pH conditions become prevalent. Movement to distal regions of the repository that remain at pressure and temperature, yet away from the buffering influence of the supercritical carbon dioxide and related processes controlled by mixed fluid equilibria (i.e., a fluid-dominated system), may return the fluid to a system of rock-dominated reactions. As neutral pH conditions prevail, silica super-saturated brine may precipitate quartz, chalcedony, or amorphous silica. The same deleterious effects that result from carbonate mineral precipitation may also take place with silica mineral precipitation, including pore plugging and repository over-pressurization that encourage carbon dioxide leakage and loss of integrity.

Nucleation and growth of siderite on shale (Fig. 7) suggests the shale is a reactive component in the system, consistent with interpretations of the aqueous compositions above. Iron cations needed for siderite precipitation derive locally from reaction between acidified brine and ferromagnesian silicate minerals. On the other hand, magnesite apparently nucleated as individual grains and splays away from specific sites on shale or arkose minerals. This relationship suggests growth of magnesite from cation-bearing brine, and only indirectly from reaction of ferromagnesian silicate minerals, similar to experiments involving high-Mg brines (Kaszuba et al., 2003). These observations are consistent with secondary carbonate precipitates in some oil fields, where siderite occurs in matrix permeability and veins are formed of calcite. Is the mode of carbonate precipitation an indication of the relative geochemical mechanisms and processes in sandstone versus shale in a carbon repository? Such contrasts in sequestration reactions may produce differing properties in the rocks. Shale reactivity may produce an increase in porosity and permeability, concomitant loss of system integrity, and potential for release of carbon dioxide. Alternatively, reactivity of the shale may yield reaction products that fill porosity and decrease permeability, thereby locally enhancing the integrity of the repository. In either case, the impact of shale reactivity on the evolving compressive and tensile strengths of the caprock, and hence the temporal structural integrity of the repository, are currently unknown.

The occurrence of a paragenetic sequence of carbonate minerals (magnesite and siderite, Figs. 6 and 7) indicates complexity of geochemical reactions among supercritical carbon dioxide, the in-place brine, the aquifer, and the aquitard. Precipitation of the mixed hydroxyl carbonate mineral dawsonite ($NaAlCO_3(OH)_2$), predicted as a stable carbonate phase in reactive transport models of carbon sequestration (Johnson et al., 2002; Knauss et al., 2002), was not observed in this study. In an effort to understand these complexities, we have calculated the saturation state of carbonate minerals (magnesite, siderite, calcite, dolomite, and dawsonite) in brine using data from Table 3. While reliable Al analyses are not available for these brines, our examination of the dataset from which Table 3 derives suggests that Al concentrations are unlikely to exceed 4 μmolal (0.1 mg/kg). In fact, more realistic Al concentrations are on the order of 0.4 μmolal (0.01 mg/kg). These calculations indicate that brine is carbonate mineral undersaturated in these experiments. However, complexities and uncertainties in the calculations (i.e., lack of experimental validation for simple mineral system reactions, limitations in activity models for brines, the effect of pressure on reaction constants, and the presence of two fluid phases) make the results primarily valuable as indicators of relative mineral stability rather than absolute stability, at this time. Evaluated in the context of relative mineral stability, dawsonite saturation brackets that of calcite and siderite, for the Al concentration range evaluated, and is lower than that of magnesite. Therefore, despite the uncertainty, these calculations usefully identify gaps in our understanding of geochemical reactions and processes within a carbon repository that are accessible for experiments and computational simulations. Important problems include adapting reaction path and reactive transport models to two-phase CO_2–

H_2O fluid systems, consistency of models with experimental observation of multi-phase fluid–rock reactions, and internal consistency of thermodynamic data for minerals identified as carbon sinks in a repository (i.e., dawsonite) (Fig. 11).

Nucleation and accelerated mineral growth of skeletal analcime took place as a consequence of carbon dioxide injection, although the phenomenological cause of this process is not constrained by our experiments. Analcime, a mineral often attributed to zeolite facies metamorphic conditions, can crystallize in a sedimentary basin or carbon repository at temperatures below 200 °C. While the high sodium activity of the brines in these experiments likely promoted analcime precipitation, analcime may also crystallize in environments with lower sodium activity. Even without crystallization of analcime, the potential for changes to mineral nucleation and growth as a response to injection of carbon dioxide, and the resulting change in the mineral fabric of the host aquifer, have significant implication for a carbon repository. In addition to filling pores, enhanced growth of pre-existing or new minerals may increase the range of grain sizes present in the aquifer. This diminished quality of grain size sorting may reduce the permeability of the aquifer. Predicative computer models do not account for changes in mineral texture, or the resulting impact of these textural changes to fluid flow in a carbon repository.

Pressure increases accompanying injection of carbon dioxide are anticipated for a carbon repository, as mirrored in our experiments. Increased pressure has been suggested as a means of repository failure due to dilation of previously sealed fractures and subsequent escape of carbon dioxide (Klusman, 2003). Plugging of pores due to precipitation of carbonate mineral may enhance the effect. Our work suggests that repository over-pressures from carbon dioxide injection may actually be somewhat alleviated by carbonate mineral precipitation but exacerbated by silica precipitation. In the dynamic reaction environment of a carbon repository, geochemically induced pressure changes will affect the integrity of a carbon repository.

In addition to the large-scale influences on the integrity of a carbon reservoir, geochemical reactions and processes identified in our experiments may provide important characteristics for monitoring and evaluation of repository performance. Silica supersaturation and increased alkalinity associated with

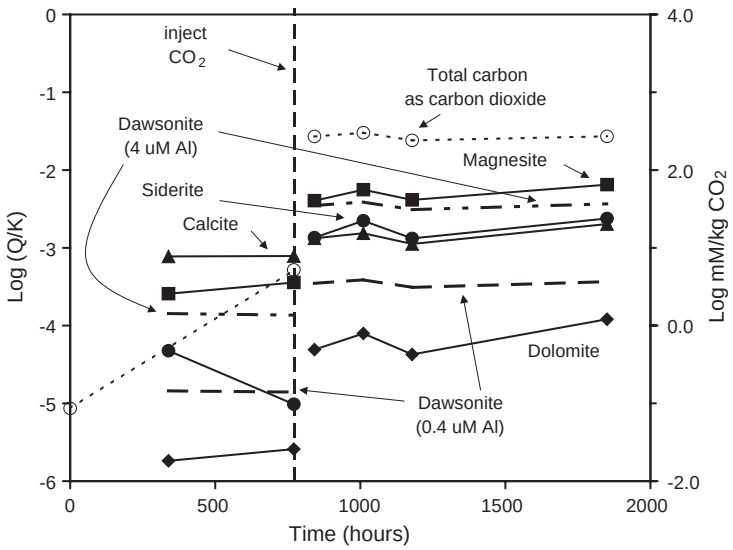

Fig. 11. Calculated saturation state of magnesite (squares), siderite (circles), calcite (triangles), and dolomite (diamonds) in supercritical CO_2–brine–rock experiment. Saturation state of dawsonite calculated for 4 and 0.4 μmolal Al is also shown (short–long dashed lines and long dashed lines, respectively). Calculations performed using Geochemist's Workbench 3.1, the resident database thermo.com.V8.R6+, and the b-dot ion association model (Bethke, 2000). Total carbon (as CO_2) during the experimental reaction is plotted as open circles and dashed lines using the scale at the right.

mixed fluid phase equilibria could be monitored as geochemical indicators in interconnected or deep-seated aquifers, springs, or water wells. Changes in these chemical parameters may provide clues to the subsurface disposition of stored carbon dioxide and may also provide new perspectives for evaluating the dynamics of existing reservoirs containing supercritical carbon dioxide.

At a minimum, this experimental study demonstrates that mixed fluid reactions and related processes have potential for geochemical reactions that have not been sufficiently addressed in the carbon sequestration literature. Fracturing, loss of system integrity, and leakage of carbon dioxide may occur just as readily as self-healing of fractures. The beneficial (or deleterious) effects, and potential impacts to repository integrity, have yet to be quantitatively identified. This rather elementary conclusion is consistent with the few studies that incorporate geochemisty into models of geologic sequestration (Gunter et al., 1997, 2000; Perkins and Gunter, 1995) and adds a vast dimension of complexity and opportunity that must be understood if geologic sequestration in a carbon repository is to be successful.

4.3. Implications for silica precipitation and quartz veins

In light of our experimental work, we suggest that multi-phase equilibrium relationships between supercritical carbon dioxide and brine–rock systems may be a source of silica cement in some sandstones and quartz mineralization in some veins. In the experimental system containing acidic brine and supercritical carbon dioxide, silica concentrations were enhanced by dissolution of silicate minerals and concomitant inhibition of the precipitation of quartz. In their evaluation of the mixing of hot hydrothermal solutions with ambient seawater at mid-ocean ridge vents, Janecky and Seyfried (1984) also noted silica super-saturation and inhibition of quartz precipitation. They attributed these phenomena to kinetics of silica polymerization and precipitation under acid pH conditions, assumptions consistent with recent experimental results (Icopini et al., 2002). Return of a silica super-saturated brine into a rock-dominated reaction system buffered to more neutral pH conditions may enhance precipitation of quartz, chalcedony, or amorphous silica as veins or cements, depending on the structure of permeability.

5. Conclusions

This experimental investigation examines geochemical reactions and processes among supercritical carbon dioxide, brine, and host rock (aquifer and aquitard) simulating a carbon repository and evaluates fluid–rock reactions that may adversely impact the integrity of the repository. The following are concluded from these experiments:

1. Addition of supercritical carbon dioxide to a brine–rock system changes the system from rock- to fluid-dominated reactions. Within a carbon repository, the carbon dioxide that is injected will exert control over geochemical reactions previously regulated or buffered by the host rock. Acid–base reactions and solubility of metals, for example, will depend on interactions between supercritical carbon dioxide and brine, with the rock reacting to these new equilibrium pressures.
2. A paragenetic sequence of carbonate mineralization (corroded magnesite and euhedral siderite) followed carbon dioxide injection. Solution composition changes, as well as nucleation and growth of siderite on shale, indicate that the aquitard will be a reactive component in a carbon repository and raises questions regarding the sequestering potential of sandstone aquifer versus shale.
3. Saturation state calculations of experimental results identify the need to adapt reaction path and reactive transport models to two-phase CO_2–H_2O fluid systems and to critically evaluate thermochemical data systems for minerals identified as potentially important carbon sinks (i.e., dawsonite).
4. Precipitation of crystalline or amorphous silica from silica–supersaturated brine and pH increase may accompany migration of fluid within and from the repository. Enhancement in silica precipitation could armor and protect flow paths or plug them.
5. Injection of carbon dioxide leads to carbonate and silicate mineral nucleation and growth. Concom-

itant change in the permeability structure of the host aquifer may adversely impact a repository.

6. In addition to direct application to geologic aquifer sequestration of carbon, an understanding of multi-phase fluid equilibrium relationships between supercritical carbon dioxide and aquifer–brine systems raises new questions and potential interpretations in a wide variety of natural geologic systems. In particular, multi-phase fluid equilibria may account for silica cement in some sedimentary basin sandstones and quartz vein mineralization in some ore districts.

Acknowledgements

Funding was provided by Los Alamos National Laboratory (LDRD/DR) for this research and by the US Department of Energy, Basic Energy Sciences, Geosciences Program for the hydrothermal laboratory facilities. Steve Chipera provided XRD analyses, Dale Counce provided brine analyses, and Emily Kluk provided XRF analyses. The final manuscript benefited from constructive comments by Eric H. Oelkers and two anonymous reviewers. This manuscript is assigned LANL LAUR # 03-2978. **[EO]**

References

Bachu, S., 2000. Sequestration of CO_2 in geological media: criteria and approach for site selection in response to climate change. Energy Convers. Manag. 41 (9), 953–970.

Bachu, S., 2002. Sequestration of CO_2 in geological media in response to climate change: road map for site selection using the transform of the geological space into the CO_2 phase space. Energy Convers. Manag. 43 (1), 87–102.

Bachu, S., 2003. Screening and ranking of sedimentary basins for sequestration of CO_2 in geological media in response to climate change. Environ. Geol. 44 (3), 277–289.

Bachu, S., Gunter, W.D., Perkins, E.H., 1994. Aquifer disposal of CO_2: hydrodynamic and mineral trapping. Energy Convers. Manag. 35 (4), 269–279.

Benson, S.M., 2000. Advances in geologic sequestration: identifying and addressing key issues. Abstr. Programs-Geol. Soc. Am. 32 (7), A200.

Bethke, C.R., 2000. The Geochemist's Workbench Release 3.1: A Users Guide. University of Illinois at Urbana-Champaign, Champaign, IL. 202 pp.

Carter, L.S., Kelley, S.A., Blackwell, D.D., Naeser, N.D., 1998. Heat flow and thermal history of the Anadarko basin, Oklahoma. AAPG Bull. 82 (2), 291–316.

Ennis-King, J., Paterson, L., 2000. Reservoir engineering issues in the geological disposal of carbon dioxide. In: Williams, D.J., Durie, R.A., McMullan, P., Paulson, C.A.J., Smith, A.Y. (Eds.), 5th International Conference on Greenhouse Gas Control Technologies, Cairns, Australia, pp. 290–295.

Gunter, W.D., Wiwchar, B., Perkins, E.H., 1997. Aquifer disposal of CO_2-rich greenhouse gases: extension of the time scale of experiment for CO_2-sequestering reactions by geochemical modelling. Mineral. Petrol. 59 (1–2), 121–140.

Gunter, W.D., Perkins, E.H., Hutcheon, I., 2000. Aquifer disposal of acid gases: modelling of water–rock reactions for trapping of acid wastes. Appl. Geochem. 15 (8), 1085–1095.

Hitchon, B., Gunter, W.D., Gentzis, T., Bailey, R.T., 1999. Sedimentary basins and greenhouse gases: a serendipitous association. Energy Convers. Manag. 40 (8), 825–843.

Holloway, S., 1997. An overview of the underground disposal of carbon dioxide. Energy Convers. Manag. 38 (SS), S193–S198.

Huffmann, E., 1977. Performance of a new automatic carbon dioxide coulometer. Microchem. J. 22 (4), 567–573.

Hurter, S.J., Pollack, H.N., 1996. Terrestrial heat flow in the Parana Basin, southern Brazil. J. Geophys. Res. 101 (B4), 8659–8671.

Icopini, G., Brantley, S., Heaney, P., 2002. Kinetics of silica nanocolloid formation from supersaturated solutions. Geochim. Cosmochim. Acta 66 (15A), A351.

Janecky, D., Seyfried, W., 1984. Formation of massive sulfide deposits on oceanic ridge crests—Incremental reaction models for mixing between hydrothermal solutions and seawater. Geochim. Cosmochim. Acta 48 (12), 2723–2738.

Johnson, J.W., Steefel, C.I., Knauss, K.G., 2002. Reactive transport modeling of geologic CO_2 sequestration. Abstr. Programs-Geol. Soc. Am. 34 (6), 390.

Kaszuba, J.P., Janecky, D.R., 2000. Experimental hydration and carbonation reactions of MgO: a simple analog for subsurface carbon sequestration processes. Abstr. Programs-Geol. Soc. Am. 32 (7), A202.

Kaszuba, J.P., Janecky, D.R., Snow, M.G., 2003. Carbon dioxide reaction processes in a model brine aquifer at 200 °C and 200 bars: implications for geologic sequestration of carbon. Appl. Geochem. 18 (7), 1065–1080.

Klusman, R., 2003. Evaluation of leakage potential from a carbon dioxide EOR/sequestration project. Energy Convers. Manag. 44 (12), 1921–1940.

Knauss, K.G., Steefel, C.I., Johnson, J.W., Boram, L.H., 2002. Impact of CO_2, contaminant gas, aqueous fluid, and reservoir rock interactions on the geologic sequestration of CO_2. Abstr. Programs-Geol. Soc. Am. 34 (6), 306.

Koide, H., et al., 1992. Subterranean containment and long-term storage of carbon dioxide in unused aquifers and in depleted natural gas reservoirs. Energy Convers. Manag. 33 (5–8), 619–626.

Lindeberg, E., 1997. Escape of CO_2 from aquifers. Energy Convers. Manag. 38 (SS), S235–S240.

Oldenburg, C.M., Pruess, K., Benson, S.M., 2001. Process modeling of CO_2 injection into natural gas reservoirs for carbon sequestration and enhanced gas recovery. Energy Fuels 15 (2), 293–298.

Perkins, E.H., Gunter, W.D., 1995. Aquifer disposal of CO_2-rich greenhouse gasses: modelling of water–rock reaction paths in a siliciclastic aquifer. In: Kharaka, Y.K., Chudaev, O.V. (Eds.), Proceedings of the 8th International Symposium on Water-Rock Interaction. A.A. Balkema, Vladivostok, Russia, pp. 895–898.

Pruess, K., Garcia, J., 2002. Multiphase flow dynamics during CO_2 disposal into saline aquifers. Environ. Geol. 42 (2–3), 282–295.

Rutqvist, J., Tsang, C., 2002. A study of caprock hydromechanical changes associated with CO_2-injection into a brine formation. Environ. Geol. 42 (2–3), 296–305.

Saripalli, P., McGrail, P., 2002. Semi-analytical approaches to modeling deep well injection of CO_2 for geological sequestration. Energy Convers. Manag. 43 (2), 185–198.

Seyfried Jr., W.E., Janecky, D.R., Berndt, M.E., 1987. Rocking autoclaves for hydrothermal experiments, II. The flexible reaction-cell system. In: Ulmer, G.C., Barnes, H.L. (Eds.), Hydrothermal Experimental Techniques. John Wiley & Sons, New York, pp. 216–239.

Span, R., Wagner, W., 1996. A new equation of state for carbon dioxide covering the fluid region from the triple-point temperature to 1100 K at pressures up to 800 MPa. J. Phys. Chem. Ref. Data 25 (6), 1509–1596.

Stein, C.L., Krumhansl, J.L., 1988. A model for the evolution of brines in salt from the lower Salado Formation, southeastern New Mexico. Geochim. Cosmochim. Acta 52, 1037–1046.

Takenouchi, S., Kennedy, G.C., 1964. The binary system H_2O–CO_2 at high temperatures and pressures. Am. J. Sci. 262, 1055–1074.

Ward's Natural Science Establishment, I., 1970. Manual for Ward's Collection of Classic North American Rocks. 45 W 7217, Rochester, NY.